Nano Research
2019, 12(5): 1129–1137
ISSN 1998-0124 CN 11-5974/O4
https://doi.org/10.1007/s12274-019-2360-5

Research Article

Polypyrrole-based hybrid nanostructures grown on textile for wearable supercapacitors

Lingchang Wang[1,2,3], Chenguang Zhang[1,2,3] (✉), Xin Jiao[1,2,3], and Zhihao Yuan[1,2,3] (✉)

[1] School of Materials Science and Engineering, Tianjin University of Technology, Tianjin 300384, China
[2] Tianjin Key Laboratory for Photoelectric Materials & Devices, Tianjin University of Technology, Tianjin 300384, China
[3] Key Laboratory of Display Materials and Photoelectric Devices, Ministry of Education, Tianjin University of Technology, Tianjin 300384, China

Received: 4 January 2019 / **Revised:** 17 February 2019 / **Accepted:** 24 February 2019

ABSTRACT

In the development of wearable energy devices, polypyrrole (PPy) is considered as a promising electrode material owing to its high capacitance and good mechanical flexibility. Herein, we report a PPy-based hybrid structure consisting of vertical PPy nanotube arrays and carbon nano-onions (CNOs) grown on textile for wearable supercapacitors. In this hybrid nanostructure, the vertical PPy nanotubes provide straight and superhighways for electron and ion transport, boosting the energy storage; while the CNOs mainly act as a conductivity retainer for the underlayered PPy film during stretching. A facile template-degrading method is developed for the large-area growth of the PPy-based hybrid nanostructures on the textile through one-step polymerization process. The fabricated stretchable supercapacitor exhibits superior energy storage capacitance with the specific capacitance of 64 $F \cdot g^{-1}$. Also, it presents the high capacitance retention of 99% at a strain of 50% after 500 stretching cycles. Furthermore, we demonstrate that the textile-based stretchable supercapacitor device can provide a stable energy storage performance in different wearable situations for practical applications. The use of the PPy-based hybrid nanostructures as the supercapacitor electrode offers a novel structure design and a promising opportunity for wearable power supply in real applications.

KEYWORDS

wearable supercapacitor, polypyrrole nanotube, carbon nano-onion, template-degrading method, stretchable electrode

1 Introduction

The development of wearable electronics has stimulated the research interests in the wearable energy storage devices to enable the integration of entire wearable systems [1–3]. Due to the advantages of high power densities, long life cycle, high safety, and easy integration with other systems, supercapacitors have drawn growing attention in the applications of wearable power supply [4–6]. For fabricating wearable supercapacitors, various substrate materials such as elastomer, paper, metallic fiber and textiles, have been used for coating electrode materials [7–10]. Among them, the textile has attractive advantages for real applications, such as light weight, porous structure for air permeability, good flexibility and adaptability to human body, and facile large-area fabrication, and thus becomes a suitable substrate for fabricating supercapacitors with scalable areas for flexible power supply of wearable electronics [11]. However, the electrode materials on textiles have to undergo repeated stretching and releasing due to the motion of human body, possibly leading to the fracture of the electrode film and the failure of the device [12]. Therefore, it is necessary to fabricate textile-based wearable supercapacitors with suitable electrode materials, which can endure stretching strain induced by human body, providing high capacitance and stable energy supply under unpredictable tensile forces.

Recently, there have been many efforts in fabricating wearable supercapacitors based on textiles with different electrode materials, including carbon-based materials, metal oxides, and conducting polymers [13]. Although carbon-based materials (e.g., carbon nanotube, graphene) have good conductivity and flexibility, they suffer from the low specific capacitance due to their intrinsic electric double layer charge storage behaviors. Metal oxides as electrode materials are capable of affording high energy storage capacitance, but their brittleness and poor conductivity limit their use in wearable supercapacitors. In the case of conducting polymers, polypyrrole (PPy), a promising candidate of flexible supercapacitor electrode material, has attracted great interests owing to its high capacitance (400–500 $F \cdot cm^{-3}$), good mechanical flexibility, and light weight, as well as the facile film preparation on the textile substrate [14, 15]. Therefore, the fabrication of PPy film on the textile is very promising for stable- and high-energy supply wearable supercapacitor electrodes.

To fabricate stretchable supercapacitors, a conformal coating film structure (with regard to the substrate) is mainly adopted, which is mostly designed into a non-coplanar buckled configuration formed by pre-straining to overcome the problem of the tensile mismatch between electrode and substrate materials [16, 17]. Usually, the stretchable substrates (e.g., polydimethylsiloxane or cloth fabric) are conformally coated by electrode materials, such as graphene, carbon nanotube, or conducting polymer film [18–20]. However, in such a conformal coating configuration, only the in-plane surface of the electrode film can be utilized, which is vertical to the preferential diffusion path of the electrolyte ions along the out-of-plane direction. Moreover, the easy aggregation of the films along the out-of-plane direction could significantly reduce the in-plane surface area. As a result, the inner space of the electrode materials cannot be fully accessed by the ions, decreasing the ion diffusion and limiting the energy storage. It has been demonstrated that the one-dimensional (1D) nanotube vertical array structure can effectively boost the

Address correspondence to Chenguang Zhang, cgzhang@tjut.edu.cn; Zhihao Yuan, zhyuan@tjut.edu.cn

energy storage performance [21, 22]. Compared to the film structure with in-plane direction paralleled to the substrate surface, the 1D vertical nanotube array structure with its longitudinal direction perpendicular to the substrate surface provides two major advantages for supercapacitor applications: (1) providing a straight superhighway along the out-of-film direction for the ions and electrons to facilitate their fast transport; (2) allowing the diffusion of electrolyte ions into the inner space of the array structure and the hollow space of the nanotubes, enhancing the surface area for energy storage [23, 24]. Therefore, if a vertical PPy nanotube array structure is utilized as the electrode for stretchable supercapacitors, the energy storage performance can be greatly improved. Usually, a flat and smooth substrate surface is required for growing the vertical nanotube array structure [25, 26]. However, textiles are porous and rough fabrics made of cylindrical-shaped fibers. So far, growing the vertical PPy nanotube array structure on textiles still remains a challenge. Moreover, an underlayer film, which is able to sustain conductivity retention under tensile forces, has to be prepared on the textile surface and underneath the vertical PPy nanotube arrays. Thus, it is highly desirable to develop a strategy to construct a vertical PPy nanotube array-based supercapacitor on textile being capable of providing stable energy supply for wearable electronic devices under stretching motions.

Herein, we demonstrate a facile template-degrading strategy for the growth of vertical PPy nanotubes on the textile substrate. In this strategy, the PPy granula (PPyG) film, which is obtained by the polymerization of Py monomer absorbed on the textile, serves as a seeded layer, while methyl orange acts as templates, conducting the growth of vertical PPy nanotubes (VPPyNTs) on the rough and porous textile substrate. The VPPyNTs are capable of enhancing the energy storage capacitance. Carbon nano-onions (CNOs), quasi-spherically nested fullerene structures with multiple graphitic layers surrounding a hollow core [27–29], were also added and encapsulated by the PPyG seeded layer film for retaining the conductivity and stabilizing the energy storage performance under tensile deformation. The resultant VPPyNT grown on the CNOs@PPyG hybrid film as an electrode structure (VPPyNTs/CNOs@PPyG) is applied to stretchable supercapacitors. The synergistic effects of the VPPyNTs and CNOs render superior stretchable performance of the solid-state device with a high specific capacitance value of 64 $F \cdot g^{-1}$, which is nearly unchanged under a stretching strain of 50% after 500 stretching cycles, and superior stretching-tolerant energy storage performance than those based on the PPyG and VPPyNTs/PPyG. Furthermore, wearable and stretchable supercapacitor-based devices have been fabricated and demonstrated to provide a stable power supply, suggesting a practical application in wearable electronics. Our work offers a strategy for preparing vertical PPy nanotube arrays on textile substrate as the stretchable supercapacitor electrode for wearable electronics.

2 Experimental

2.1 Materials

Pyrrole (Py), iron chloride hexahydrate, 2,6-naphthalenedisulfonic acid disodium, methyl orange, phosphoric acid and poly (vinyl alcohol) (PVA) were commercially obtained from Shanghai Aladdin Bio-Chem Technology Co., LTD. The pyrrole monomer was distilled under reduced pressure before use. CNOs were prepared according to our previous report [30]. The spandex fabric was purchased for the textile substrate.

2.2 Preparation of stretchable electrodes

The VPPyNTs/PPyG structure on textile (VPPyNTs/PPyG-textile) was synthesized by a facile self-degraded template method through a one-step chemical oxidation process. Firstly, the spandex fabric was ultrasonically cleaned with deionized (DI) water and ethyl alcohol, followed by soaking in 0.4 M of NaOH solution and washing with DI water to neutral. Then a piece of spandex fabric with an area of 2.7 cm × 2 cm was pre-strained to 3.4 cm along its length direction and its two edges were fixed on a glass substrate by clamps. 0.075 mL of Py/methanol mixture solution (volume ratio of Py to methanol = 2:5) was then dropped onto the pre-strained spandex fabric and kept at a temperature of 0–4 °C for 30 min. After that, 1 mL of methyl orange solution (5 mM) was dropped onto the spandex fabric, which was kept at the same temperature for another 10 min. 50 mL of oxidizer solution (prepared by dissolving 8 g iron chloride hexahydrate and 0.1296 g 2,6-naphthalenedisulfonic acid disodium in 100 mL of DI water with 0.3 M of hydrochloric acid) was then slowly dropped onto the above spandex fabric [31]. After 5 h, the spandex fabric was taken out, rinsed with DI water and dried. As a comparison, the PPy film structure on textile (PPyG-textile) was also synthesized using the same conditions without methyl orange. The VPPyNTs/CNOs@PPyG composite structure on textile (VPPyNTs/CNOs@PPyG-textile) was synthesized using the same process but the CNOs are dispersed in the oxidizer solution (CNO concentration = 0.03 $mg \cdot mL^{-1}$) and added into the PPy structures during the polymerization process [32]. After synthesis, rinsing and drying, the pre-strained fabric was released from the glass substrate and employed for the subsequent stretchable supercapacitor assembling.

2.3 Fabrication of stretchable supercapacitor

The solid-state stretchable supercapacitor was fabricated by assembling the above PPy-textile electrodes and a gel electrolyte into a sandwiched structure. The gel PVA/H_3PO_4 electrolyte was prepared as follows: 3 g of PVA powder was mixed with 30 mL of DI water and heated to 85 °C under vigorous stirring until the solution became clear. 4.5 g of H_3PO_4 was then added into the above solution and stirred for 1 h [33]. After cooling to room temperature, the gel electrolyte was placed between the two electrodes and dried at room temperature to solidify. Finally, the stretchable supercapacitor was obtained and ready for electrochemical measurements. The wearable supercapacitor for powering an electronic watch was fabricated by connecting four VPPyNTs/CNOs@PPyG supercapacitors in series. In detail, five pieces of the VPPyNTs/CNOs@PPyG-textiles with an area of 3 cm × 5 cm were employed for connection. Three of them were coated by the gel electrolyte on their two edges with a coating area of 1.25 cm × 5 cm, while another two were coated by the gel electrolyte only on one edge. Then, the electrolyte-covered areas were overlapped with each other in sequence of end-to-end to construct four supercapacitors connected in series, wherein the parts without electrolyte coating serve as the electronic connection between the supercapacitors. Copper tapes were attached onto the edges of the entire supercapacitor device to serve as current collectors. Finally, the device was attached onto the watchband and connected to the watch electrodes by copper wires to work as a wearable supercapacitor.

2.4 Materials characterization

The morphologies and structures of the PPy structures were characterized by a scanning electron microscope (SEM, JEOL JSM-6700F) and a transmission electron microscope (TEM, JEM-2100F), respectively. The contour map of Joule heat distribution was captured by a HT-02 type infrared camera. The chemical compositions were examined by Fourier transform infrared (FTIR) spectroscopy (Frontier Mid-IR FTIR) and X-ray photoelectron spectroscopy (XPS, ESCALAB250Xi). The compositions of the samples were identified by X-ray diffraction (XRD, Rigaku D/max-2500/PC). Electrochemical measurements were carried out using electrochemical workstations (ZAHNER-Thales). Electrochemical impedance spectroscopy (EIS) measurements were carried out in the frequency range of 0.1 Hz to

100 kHz at an open-circuit potential. The cycling stability was measured in a Land 2001A battery test system. Electrochemical measurements of the stretchable supercapacitor were conducted by fixing two edges of the electrode and moving along its length direction in a WDW-02 type electronic universal testing machine.

3 Results and discussion

The PPy-based hybrid nanostructures on textile, including VPPyNTs/PPyG and VPPyNTs/CNOs@PPyG, were synthesized by a facile template-degraded method through one-step polymerization process, as illustrated in Fig. 1(a). Spandex fabric was chosen as the textile substrate due to its good elasticity and stretchability, a piece of which was pre-strained and fixed on a glass substrate, followed by adding Py monomer and methyl orange solution in sequence. The growth mechanism of the VPPyNTs/PPyG on textile can be interpreted as follow: When iron (III) chloride solution was dropped onto the spandex fabric pre-coated with Py monomer and methyl orange, fibrous precipitates were formed into vertical array templates due to the complexation interaction between Fe^{3+} and methyl orange [34]. Meanwhile, induced by the Fe^{3+} oxidizer, the polymerization reaction occurred to form the PPyG film coating on the surface of the fabric and vertical fibrillar templates, during which Fe^{3+} was gradually reduced to Fe^{2+}, leading to the degradation and disappearance of the fibrillar templates with no need of purification. During the one-step polymerization process, the PPyG film and the above-grown VPPyNTs were simultaneously formed on the fabric surface, and the PPyG film serves as an intermediate layer between the VPPyNTs and the textile substrate. To synthesize the VPPyNTs/CNOs@PPyG on textile, the CNOs were deposited on the fabric surface by adding the CNOs/$FeCl_3$ mixture solution during the polymerization, and then encapsulated in the PPyG film to form the hybrid structure. To synthesize the PPyG film on textile, the same synthesis procedure was carried out without adding methyl orange and CNOs. After synthesis, the fabric was released to its original length for the application in the stretchable supercapacitor electrode. In order to verify the feasibility of this method in preparing wearable electrodes for practical applications, the electrode of VPPyNTs/CNOs@PPyG on textile with a large area of 16 cm × 14 cm has been fabricated, as shown in Figs. 1(b) and 1(c). A contour map of the surface temperature shown in Fig. 1(e) demonstrates that a uniform temperature distribution was obtained under an input voltage of 5 V, indicating the uniform formation of the PPy nanostructures on the textile surface. The adhesion test by peeling off the scotch tape from the PPy on the textile surface was also carried out. As shown in Fig. 1(d), there is no black powder remaining on the lower surface of the tape, demonstrating that the PPy cannot be easily removed from the fabric surface. The strong combination between the PPy and the fabric surface can be attributed to the hydrogen bonding formation between the amino groups of fabric and nitrogen atoms in pyrrole, which is beneficial for achieving the stable performance in the application of stretchable and wearable energy storages.

SEM images of the pristine textile, PPyG-textile, VPPyNTs/PPyG-textile, and VPPyNTs/CNOs@PPyG-textile were shown in Figs. 2(a)–2(d). The pristine spandex fabric has a smooth surface (Fig. 2(a)). After growing PPyG film, the surface became rough (Fig. 2(b)), which consists of interconnected PPy granula (shown in Fig. S1(a) in the Electronic Supplementary Material (ESM)). From Fig. 2(c), the VPPyNTs have a high growth density on the fabric surface. In the case of the VPPyNTs/CNOs@PPyG composite structure, the growth of VPPyNTs structures on the fabric surface can also be observed (Fig. 2(d)), suggesting that the addition of the CNOs has no influence on the product morphology. The insets in Figs. 2(c) and 2(d) show the TEM images of PPy nanotubes in the VPPyNTs/PPyG-textile and the VPPyNTs/CNOs@PPyG-textile, respectively. The PPy nanotubes have a hollow structure, which is formed by the degradation of the encapsulated template during the polymerization process. Figure 2(e) and Fig. S1(b) in the ESM show the magnified SEM images of VPPyNTs, in which VPPyNTs with an average diameter of 200 nm and length of 1 μm were grown on the PPyG film coating on the fabric surface in vertical directions instead of random directions, rendering them an enhanced energy storage performance. TEM characterization is carried out to further examine the PPy nanotube structure. Figure S1(c) in the ESM shows that a typical PPy nanotube has a diameter of ~ 200 nm and an inner space diameter of ~ 40 nm. The high-resolution TEM (HRTEM) image shown in Fig. 2(f) shows that the PPyG film in the VPPyNTs/PPyG-textile is grown with an amorphous structure. CNOs were added and used as conductivity retainer to interconnect the adjacent PPy particles in the PPyG film during the stretching of the electrode. As can be seen in Fig. 2(g), CNOs have typical structures of spherical graphitic layers surrounding a hollow space, and the particle sizes range from 20 to 30 nm. In our case, CNOs can be homogeneously dispersed in the $FeCl_3$ aqueous solution, enabling a uniform distribution and encapsulation of the CNOs in the PPyG film (Fig. S1(e) in the ESM). After hybridizing with the CNOs, the PPyG film became more crystallized, as indicated in Fig. 2(h) and Fig. S1(g) in the ESM. The crystalline structure with a lattice spacing of 0.35 nm can be clearly observed in the TEM image (Fig. 2(h)), demonstrating that the CNOs have been uniformly encapsulated in the PPyG film. Figures S1(h) and S1(i) in the ESM show that the PPy nanotubes in both VPPyNTs/PPyG-textile and VPPyNTs/CNOs@PPyG-textile structures have an amorphous structure. Based on these results, it can be concluded that the CNOs were mainly incorporated into the PPyG film rather than the vertical PPy nanotubes. Thus, the CNOs can be preferentially absorbed onto

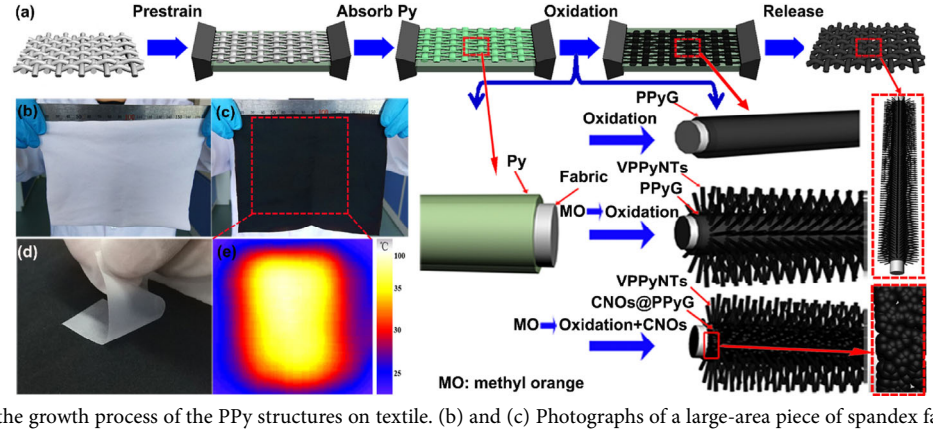

Figure 1 (a) Schematic of the growth process of the PPy structures on textile. (b) and (c) Photographs of a large-area piece of spandex fabric (16 cm × 14 cm) before and after the growth of the PPy structures. (d) Photograph of the adhesion test on the PPy-textile electrode. (e) Contour map of the surface temperature distribution in a square region in the PPy-textile electrode in (c) under an input voltage of 5 V.

the fabric surface instead of the fibrous precipitate templates due to the gravity and larger surface area of the fabric. Simultaneously, the CNOs can easily combine with the pre-coated Py monomer due to the π–π interaction, facilitating the encapsulation of the CNOs in the PPyG film during the subsequent polymerization [35]. The encapsulation of the CNOs in the PPyG film can strengthen the interconnections between the adjacent PPy particles and keep the electron transport paths continuous in the PPyG film under stretching. FTIR characterization is conducted to examine the chemical compositions of the as-synthesized PPy structures (Fig. 2(i)). As can be observed, C=C and C–N stretching vibrations of pyrrole molecular ring at peaks of 1,540 and 1,460 cm^{-1}, C–H in-plane vibration at peaks of 1,316 and 1,030 cm^{-1}, and C–H out-of-plane vibration at the peak of 910 cm^{-1} are characteristic peaks of PPy [36–38], consistent with the previous reports. There is no shift in the peak positions in the PPyG, VPPyNTs/PPyG, and VPPyNTs/CNOs@PPyG, indicating that the VPPyNTs and CNOs have no effect on the characteristic peak positions of the PPy. XRD patterns of the three PPy structures are shown in Fig. 2(j). Broad characteristic peaks appear in the same positions between 20° and 30° in the three samples, indicating that all the PPy structures are amorphous [39]. Compared to the PPyG and VPPyNTs/PPyG, the VPPyNTs/CNOs@PPyG has more crystallized structure. The increased crystallization can be attributed to the presence of the highly graphitized CNOs in the hybrid structure, as indicated by the XRD pattern and TEM image in Fig. S2 in the ESM. Figure 2(k) shows the XPS spectra of the three PPy structures. The presence of C 1s (284.8 eV), N 1s (399.8 eV), and O 1s (531.3 eV) peaks in the full survey spectra further demonstrates the PPy with high purity [40].

The effects of methyl orange concentration on the PPy structures and the corresponding electrochemical properties were studied. Figure S3 in the ESM shows the different PPy nanostructures on textile by using different methyl orange concentrations during synthesis. As can be observed, the growth density of the PPy nanotubes increases with an increase of the methyl orange concentration. Specifically, the VPPyNTs structures were obtained on textile at methyl orange concentrations ranging from 3 to 5 mM, and higher methyl orange concentration results in a longer average tube length. When the concentration increases to 10 mM, the PPy nanotubes grow into random directions and get entangled with each other. The dependence of the electrochemical performance of the PPy-textile structures on their morphologies was also studied. Figures S4(a) and S4(b) in the ESM show that the highest specific capacitance was obtained from the PPy-textile structure synthesized at a methyl orange concentration of 5 mM. This is understandable as the VPPyNTs structure provides facile access for ions and straight path for electron transport, whereas the entangled PPy nanotubes reduce the accessible area for ions, and electrons have to transport along curved nanotube pathways. Therefore, the methyl orange concentration of 5 mM was chosen as the optimal concentration to carry out the synthesis of VPPyNTs structures on the textile.

To confirm the merits of the VPPyNTs structure in the supercapacitor electrode, the electrochemical properties of the PPyG-textile and the VPPyNTs/PPyG-textile were investigated in a three-electrode system with 1 M KCl aqueous solution. Figure 3(a) shows the cyclic voltammetry (CV) curves of the two structures at a scan rate of 5 $mV \cdot s^{-1}$, both of which demonstrate the typical pseudo-capacitive behavior [31]. The CV curve of the VPPyNTs/PPyG-textile has a larger enclosed area than that of the PPyG-textile, indicating the larger specific capacitance. Figure 3(b) shows the galvanostatic charge–discharge (GCD) curves of these two structures at a current density of 0.5 $A \cdot g^{-1}$. The specific gravimetric capacitance (C_m) values of the two structures with respect to the discharge current densities were calculated according to the GCD curves and plotted in Fig. 3(c). The calculated C_m for the VPPyNTs/PPyG-textile is 475 $F \cdot g^{-1}$, much higher than that of the PPyG-textile (294 $F \cdot g^{-1}$). From Fig. 3(c), the VPPyNTs/PPyG-textile has larger specific capacitance than the PPyG-textile at various current densities. The main reason is that compared to the PPyG structure, the VPPyNTs/PPyG is capable to provide not only a straight superhighway along the out-of-film direction for the ions and electrons to facilitate their fast transport, but also a large surface area for electrolyte ion access and charge storage. This is also consistent with the results in Fig. S4 in the ESM. Figure 3(d) shows the Nyquist plots of the two structures characterized by the EIS. A semicircle appears in the higher frequency region, and a nearly straight line appears in the lower frequency region. The first intersection of the semicircle with Z' real axis represents the equivalent series resistance (R_s), which results from the contact

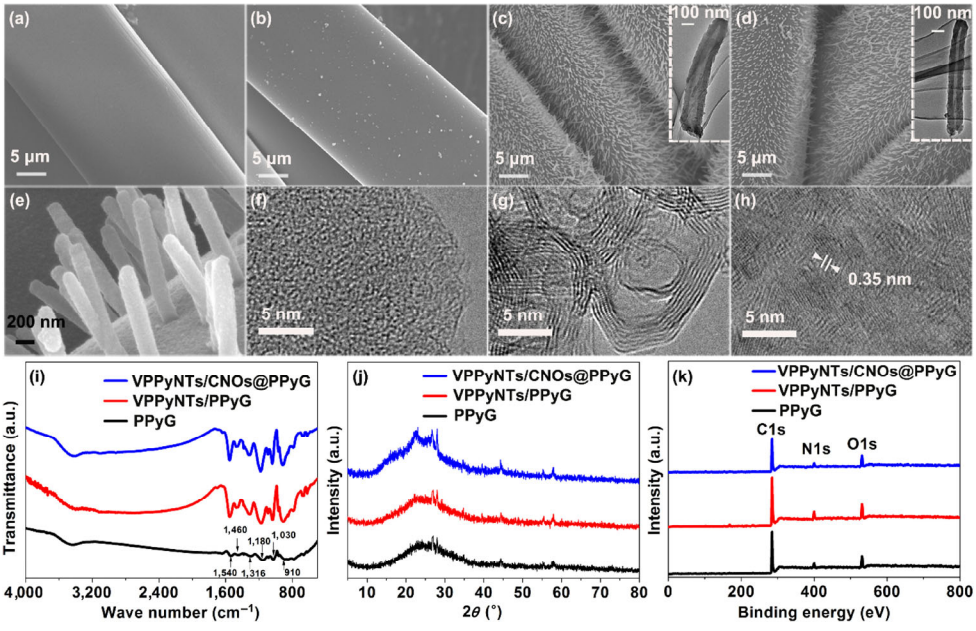

Figure 2 SEM images of (a) pristine textile, (b) PPyG-textile, (c) VPPyNTs/PPyG-textile, and (d) VPPyNTs/CNOs@PPyG-textile. The insets in (c) and (d) show TEM images of PPy nanotubes in the corresponding structure. (e) Magnified SEM image of the VPPyNTs. (f) HRTEM image of the underlayered PPy film in the VPPyNTs/PPyG structure. (g) HRTEM image of CNOs; (h) HRTEM image of the PPy film in the VPPyNTs/CNOs@PPyG composite structure. (i) FTIR spectra, (j) XRD patterns, and (k) XPS full survey spectra of the PPyG, VPPyNTs/PPyG, and VPPyNTs/CNOs@PPyG.

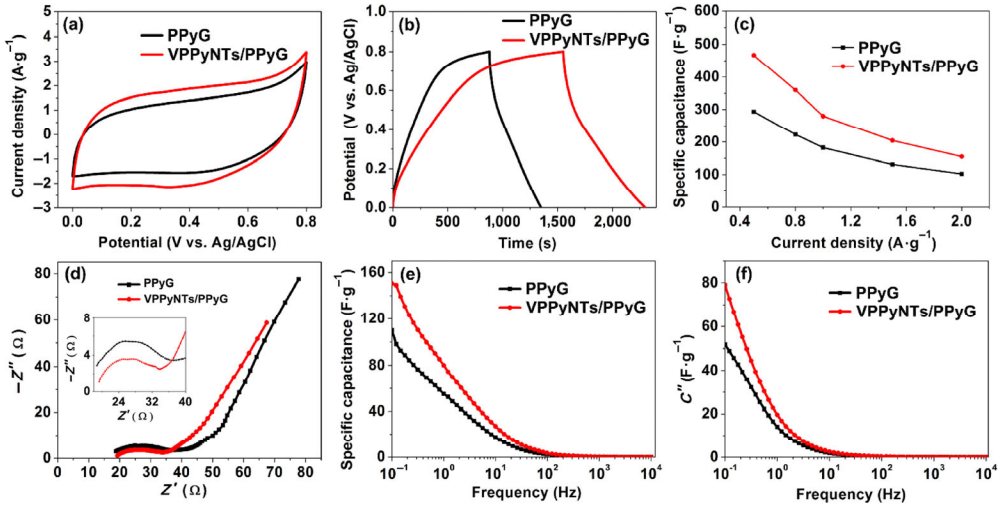

Figure 3 Electrochemical properties of the PPyG-textile and VPPyNTs/PPyG-textile measured by a three-electrode system using 1 M KCl aqueous solution: (a) CV curves at a scan rate of 5 mV·s^{-1}; (b) GCD curves at a current density of 0.5 A·g^{-1}; (c) plots of specific gravimetric capacitances versus different current densities; (d) Nyquist plots measured in the frequency range of 0.1 Hz to 100 kHz; (e) and (f) frequency response of the specific capacitance (e) and C'' (f).

resistance between the electrode and electrolyte interface, the intrinsic resistance of the electrode material, and the sum resistance of the electrolyte [41]. The semicircle is ascribed to the charge transfer resistance (R_{ct}), and a small diameter indicates a low R_{ct} and the resulting high charge transfer rate [42]. From the Nyquist plots, the VPPyNTs/PPyG-textile has much lower R_s and R_{ct} than the PPyG-textile (inset in Fig. 3(d)). During the synthesis process, the VPPyNTs were grown vertically with space among the nanotubes from the PPyG film on the surface of the pre-strained spandex fabric. After releasing, the shrunk fabric will result in the shrinkage of space and the possible contact of PPy nanotubes with each other. Thus, the VPPyNTs/PPyG-textile has a higher conductivity than the PPyG-textile. CV curves of the PPyG-textile, VPPyNTs/PPyG-textile, and VPPyNTs/CNOs@PPyG-textile structures at different scan rates are shown in Figs. S5(a)–S5(c) in the ESM. The VPPyNTs/CNOs@PPyG-textile has a better shape retention than the VPPyNTs/PPyG-textile and a higher current density than the PPyG-textile at higher scan rates. This indicates that the presence of the CNOs can improve the rate capability of the PPy structures. Figures S5(d) and S5(e) in the ESM show that the VPPyNTs/CNOs@PPyG-textile has lower and higher C_m than the VPPyNTs/PPyG-textile at lower and higher discharge current densities, respectively, suggesting a better rate capability. The Nyquist plots in Fig. S5(f) in the ESM show that the VPPyNTs/CNOs@PPyG-textile has the lowest R_{ct} among the three PPy nanostructures on textile, which can be attributed to the increased conductivity of the PPyG film after adding CNOs. Furthermore, the advantages of the VPPyNTs/PPyG-textile in energy storage have also been demonstrated by the response dependence of specific capacitance and imaginary capacitance (C'') on the frequency. According to the bode plots in Fig. 3(e), the VPPyNTs/PPyG-textile has higher C_m than that of the PPyG-textile at low frequency, which can be attributed to its higher specific surface area [43]. Figure 3(f) shows that the VPPyNTs/PPyG- textile has higher C'' than the PPyG-textile, indicating a more rapid charge transport, which is benefited from the straight superhighways paralleled to the electron and ion transport provided by the vertical nanotube structure [44]. The above-mentioned results confirm the advantages of the VPPyNTs as the supercapacitor electrode material for enhanced energy storage applications.

The advantages of the supercapacitor based on the VPPyNTs/CNOs@PPyG-textile electrodes in stretchable energy storage were further studied. The effect of the CNO content on the electrochemical property of the hybrid structure was investigated by the three-electrode system measurements. The VPPyNTs/CNOs@PPyG-textile electrodes with different CNO contents have been synthesized, and the solid-state supercapacitors were also assembled by sandwiching the PVA/H_3PO_4 gel electrolyte between two symmetric electrodes. Since the VPPyNTs/CNOs@PPyG-textile with a CNOs content of 0.03 mg·mL^{-1} has the highest C_m (Fig. S6 in the ESM), the sample with the CNO content of 0.03 mg·mL^{-1} was chosen for the following studies. Figure 4(a) shows the CV curves of the supercapacitors based on the PPyG-textile and the VPPyNTs/CNOs@PPyG-textile at a scan rate of 5 mV·s^{-1}, and Figs. S7(a)–S7(c) in the ESM show those at different scan rates. It can be seen that the solid-state supercapacitor based on VPPyNTs/CNOs@PPyG-textile electrodes has the specific capacitance of 64 F·g^{-1}, which is 2.2 times of that based on the PPyG-textile electrodes (29 F·g^{-1}). This further demonstrates that the VPPyNTs structure as the electrode material has the advantage in boosting energy storage for supercapacitor applications. The Nyquist plots given in Fig. 4(b) show that the stretchable supercapacitor based on the VPPyNTs/CNOs@PPyG-textile electrodes has a much lower R_s ($\leq$ 250 Ω) than that of the device based on the PPyG-textile electrodes ($\geq$ 350 Ω). Thus, the addition of CNOs increases the conductivity of the PPyG film in the VPPyNTs/CNOs@PPyG-textile. The cycling stability of the solid-state supercapacitors was also evaluated by measuring GCD cycles at a current density of 0.3 A·g^{-1}. As shown in Fig. 4(c), after 1,000 GCD cycles, the supercapacitor based on the VPPyNTs/CNOs@PPyG-textile retains 85% of the initial specific capacitance, while those based on the VPPyNTs/PPyG-textile and PPyG-textile have the capacitance retention of 69% and 59%, respectively. The comparison of GCD curves of the supercapacitors based on the three PPy-textile structures can be found in Fig. S7(d) in the ESM, and the stretchable supercapacitor based on the VPPyNTs/CNOs@PPyG-textile was calculated to deliver an energy density of 5.7 Wh·kg^{-1}. Figure S7(e) in the ESM shows the plots of the capacitance retention of the supercapacitors based on three PPy-textile structures during the electrochemical cycling. It is seen that without adding CNOs, the PPy nanostructures exhibited poor cycling stability due to the swelling and shrinking of the PPy particles coming from the doping and de-doping of anions in the PPy backbone. The volume change will lead to the structural pulverization, which is responsible for the performance degradation [45]. It has been reported that adding CNOs can increase the cycling stability of the conducting polymers [46]. The spherical graphitic structure is capable of depressing the volume change due to the π–π interaction between the CNOs and PPy. In addition, the space among the PPy nanotubes can accommodate their volume change [47]. As a result, the supercapacitor based on the VPPyNTs/

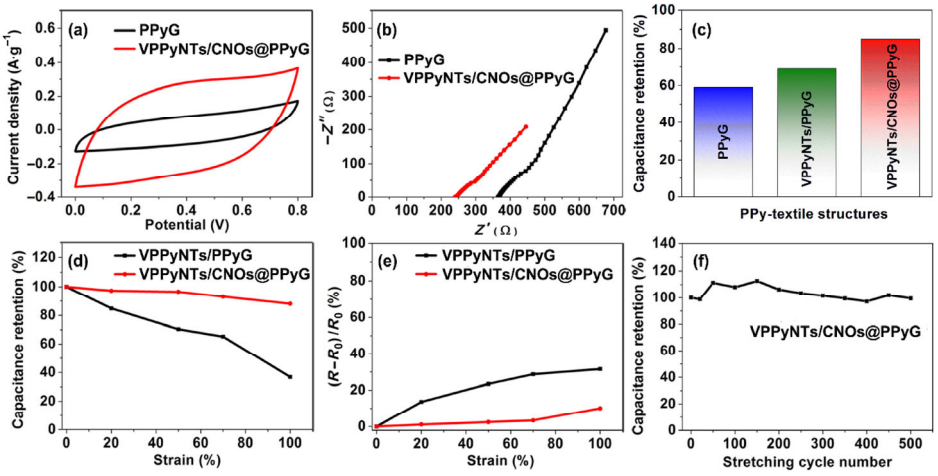

Figure 4 (a)–(c) Electrochemical performance of the solid-state supercapacitors based on the PPyG-textile and the VPPyNTs/CNOs@PPyG-textile electrodes: (a) CV curves at a scan rate of 5 mV·s^{-1}; (b) Nyquist plots measured in the frequency range of 0.1 Hz to 100 kHz; (c) comparison of capacitance retention after 1,000 charge–discharge cycles measured at a current density of 0.3 A·g^{-1}. (d)–(f) Stretchable supercapacitor performance of the solid-state supercapacitors based on the VPPyNTs/PPyG-textile and the VPPyNTs/CNOs@PPyG-textile electrodes: (d) capacitance retention under different strains; (e) resistance retention under different strains; (f) capacitance retention of the solid-state supercapacitor based on the VPPyNTs/CNOs@PPyG-textile electrodes after 500 stretching cycles under a strain of 50%.

CNOs@PPyG-textile has a superior cycling stability than those based on the VPPyNTs/PPyG-textile and PPyG-textile. The increased capacitance retention during the electrochemical cycling can be ascribed to the electrochemical activation [48]. The GCD curve of the supercapacitor based on the VPPyNTs/CNOs@PPyG-textile still remains a triangle shape in the last 10 cycles (Fig. S7(f) in the ESM), indicating high Coulombic efficiency and stable electrochemical performance of the hybrid structure. The C_m value of our stretchable supercapacitor based on the VPPyNTs/CNOs@PPyG-textile is higher than those reported in previous studies, as listed in Table S1 in the ESM.

For the applications of stretchable supercapacitors, it is necessary to have good capacitance retention of the electrode materials under stretching. Thus, the capacitance retention of the supercapacitor devices under different strains were studied. Figure 4(d) shows the capacitance retention variations of the supercapacitors based on the VPPyNTs/PPyG-textile and VPPyNTs/CNOs@PPyG-textile with changing their stretching strains. The supercapacitor based on the VPPyNTs/PPyG-textile keeps decreasing with an increase of the strain. In contrast, the one based on the VPPyNTs/CNOs@PPyG-textile has no obvious capacitance change when the strain is below 50%, and still remains a retention ratio of 88% at a strain of 100%, much higher than that based on the VPPyNTs/PPyG-textile (37%). These results can be further demonstrated in Fig. S8 in the ESM, which shows the CV curves of the supercapacitors based on different PPy-textile structures at a scan rate of 5 mV·s^{-1} under different strains. To interpret the superior and stable performance of the stretchable supercapacitor based on the VPPyNTs/CNOs@PPyG-textile, we examined the resistance variations of different PPy nanostructures on textile under different strains. Figure 4(e) shows that the VPPyNTs/CNOs@PPyG-textile electrode has a resistance increase of less than 4% upon an increased strain of 70% (the photographs of the VPPyNTs/CNOs@PPyG-textile electrodes at its original length and under a stretching strain of 100% are shown in Fig. S9 in the ESM). In contrast, the VPPyNTs/PPyG-textile electrode has a resistance increase of larger than 27% when subjected to the same strain. The sheet resistance variations of the three PPy-textile electrodes were also measured under different strains (the sheet resistance calculation method is described in the ESM). Figure S10 in the ESM shows that the sheet resistance of the VPPyNTs/CNOs@PPyG-textile electrode barely changes during the stretching, whereas the other two PPy-textile electrodes undergo obvious changes. Therefore, it can be concluded that the capacitance retention performance of the stretchable supercapacitor is mainly correlated to their resistance retention during stretching. The better resistance retention of the VPPyNTs/CNOs@PPyG-textile as the stretchable electrode can be ascribed to the connection of the PPy particles by the CNOs dispersed in the PPyG film, which renders the electrode better capacitance retention in the stretchable supercapacitor application. Moreover, the electrochemical stability of the stretchable supercapacitor based on the VPPyNTs/CNOs@PPyG-textile was examined after multiple stretching cycles. Figure 4(f) shows that after stretching for 500 cycles at a strain of 50%, the capacitance retention is still higher than 99%, indicating its excellent electrochemical stability under stretching. Consequently, the stretchable supercapacitor based on the VPPyNTs/CNOs@PPyG-textile has superior properties in both energy storage and capacitance retention. Table S1 in the ESM lists the performance of the stretchable supercapacitors in our work and previous reports. It can be seen that the VPPyNTs/CNOs@PPyG hybrid structure in our work has the highest specific capacitance and capacitance retention under stretching. These all demonstrate the advantages of the VPPyNTs/CNOs@PPyG hybrid structure in the application of stretchable supercapacitors.

From the above results, the mechanism of the superior performance of the stretchable supercapacitor based on the VPPyNTs/CNOs@PPyG-textile is proposed. To synthesize the VPPyNTs/PPyG-textile and PPyG-textile structures, the same amount of pyrrole monomer was used. In the former case, the pyrrole monomer was used to synthesize both the VPPyNTs and the PPy film; while in the latter case, all the pyrrole monomer was used to synthesize the PPy film. As a result, a much thinner PPy film was formed in the VPPyNTs/PPyG-textile than that in the PPyG-textile structure. The conductivity of the PPy structure as the stretchable supercapacitor electrode during stretching is mainly maintained by the PPyG film formed on the fabric surface. Due to its thin thickness, the PPyG film in the VPPyNTs/PPyG structure will be easily broken during stretching, which will significantly degrade the capacitance retention during stretching.

To maintain the performance of the VPPyNTs/PPyG-textile structure as the stretchable supercapacitor electrode, two approaches can be employed. One method is to increase the thickness of the PPyG film by adding more pyrrole monomer, which will increase the electrode mass and compromise the device performance [24]. The other one is to improve the conductivity of the PPyG film through hybridizing with highly conductive carbon materials. Graphene

with a large 2D surface area and carbon nanotubes with a high 1D aspect ratio can hardly be easily dispersed in $FeCl_3$ aqueous solution. Thus, they might form large aggregates on the fabric surface due to the large van der Waals interaction and degrade the stretchable supercapacitor performance. Moreover, graphene and carbon nanotubes will absorb large amount of Fe^{3+} cations due to their large surface areas and might affect the formation of the fibrous methyl orange-Fe^{3+} templates. By comparison, the quasi-zero-dimensional (0D) CNOs can be easily dispersed in aqueous solution and deposited homogeneously on the fabric surface. The smaller surface area of the CNOs makes them absorb less Fe^{3+} cations, resulting in less influences on the formation of the fibrous templates. Figure S11 in the ESM shows that obvious fracture will occur in the thin PPyG film in the VPPyNTs/PPyG-textile structure upon the initiation of stretching. The density and size of the fractures become larger as the stretching strain increases from 0 to 100%. The PPy particles will be disconnected in these local fractured areas, breaking the electron transport paths and increasing the resistance. In contrast, no obvious fracture is observed on the surface of the PPyG film in the VPPyNTs/CNOs@PPyG-textile structure when increasing the stretching strain (Fig. S12 in the ESM), since the CNO nanoparticles are homogeneously distributed inside (Fig. S1(e) in the ESM). As the strain increases, along the stretching direction stress is transferred by the CNOs, which bridge the adjacent PPy particles, postponing the crack generating and propagating. Moreover, the spherical CNO structure can relieve the stress concentration in the PPyG film during stretching and electrochemical cycling, providing a maximum avoidance of the fractures. Thus, the electron transport pathways are retained to the maximum extent and a high conductivity retention ratio is kept during stretching. The above discussion was schematically illustrated in Scheme 1. The PPy structure herein as the stretchable supercapacitor electrode plays dual roles as both the current collector and the energy storage material. The volume change of the PPy caused by the ion doping and de-doping will lead to the resistance increase and the electrochemical performance degradation. The CNOs in the VPPyNTs/CNOs@PPyG-textile structure will not only compensate the conductivity loss of the PPyG film as the current collector, but also improve the electrochemical stability of the PPy as the energy storage material [32]. Moreover, CNOs with a hollow structure can boost the energy storage capacitance due to the ion accommodation in the inner void space [49]. It has been reported that the thin electrode film is beneficial for the rapid electrochemical response and enhanced storage capacity [50]. However, as the stretchable supercapacitor electrode, the thin film will be easily broken, leading to the failure of the device. This problem can be solved in our work by hybridizing with the CNOs in the PPyG film. In the VPPyNTs/CNOs@PPyG-textile structure, the CNOs@PPyG hybrid film mainly acts as the good stretchable current collector, while the VPPyNTs vertically grown on it mainly act as the energy storage capacity enhancer. Our study thus provides a reference for the rational design of the vertical nanotube array-based structure for stretchable supercapacitor applications, as well as using and optimizing thin film structure as the stretchable supercapacitor electrode.

In practical applications, it is necessary to connect multiple supercapacitors in series or parallel to meet the high voltage or current demand of the electronic equipment. As a demonstration, stretchable supercapacitors composed of two, three, and four single devices based on the VPPyNTs/CNOs@PPyG-textile connected in series and parallel were fabricated. As the corresponding CV and GCD curves shown in Figs. 5(a) and 5(b), the supercapacitors composed of two, three, and four devices in series exhibit enhanced operating potentials, which are 2, 3, and 4 times of a single one, respectively. Also, the supercapacitors composed of two, three, and four devices in parallel show increased output currents, which are 2.2, 3.7, and 4.2 times of a single one, respectively. The integrated supercapacitor device can light up a red light-emitting diode (Re-LED, 2.2 V) under a stretching strain of 50%, and there is almost no intensity change compared to its original state (Figs. 5(c) and 5(d)), indicating its potential application in the stretchable energy storage. The applications of the integrated supercapacitor device as wearable power supply were further studied. Figure 5(e) shows that the Re-LED can be lighted up by the stretchable supercapacitor attached on the human hand and finger, and the intensity change is unnoticeable under the bending states compared to the original state of the device. Also, the supercapacitor device can work under both the stretching and twisting states, and the light intensity of the Re-LED keeps almost unchanged (Fig. 5(f)). Moreover, the integrated stretchable supercapacitor can also be used as a power source to drive an electronic watch to run for several minutes (Fig. 5(g)). These demonstrate that the VPPyNTs/CNOs@PPyG-textile structure is promising in the applications in wearable power supply and electronics.

4 Conclusions

In summary, we have synthesized the vertical PPy nanotube array structure on the textile and employed it as the electrode material in the application of stretchable supercapacitors. The VPPyNTs/PPyG structure was grown on the textile by a facile template-degrading method through a one-step polymerization process, while the CNOs were added into the PPyG film during the synthesis to form the hybrid structure. The solid-state supercapacitor assembled by the VPPyNTs/CNOs@PPyG-textile structure exhibits the high specific capacitance of 64 $F \cdot g^{-1}$, which is nearly unchanged after stretching for 500 cycles at a strain of 50%, as well as a high capacitance retention ratio of 88% at a strain of 100%. In this stretchable electrode structure, the VPPyNTs provide straight superhighways for fast electron transport and an enhanced surface area for charge storage, while the CNOs retain the conductivity and stabilize the electrochemical performance of the PPy film during stretching. The synergistic effect leads to the superior performance in stretchable energy storage than the devices based on the PPyG and VPPyNTs/PPyG structures. Furthermore, the potential use of the VPPyNTs/CNOs@PPyG structure for wearable power supply has been demonstrated by the stable

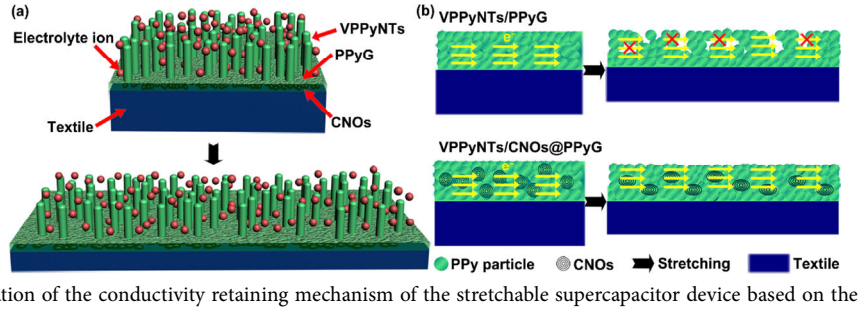

Scheme 1 (a) Schematic illustration of the conductivity retaining mechanism of the stretchable supercapacitor device based on the VPPyNTs/CNOs@PPyG-textile electrode during stretching. (b) Schematic illustration of structural evolutions of the VPPyNTs/PPyG-textile electrode and the VPPyNTs/CNOs@PPyG-textile electrode.

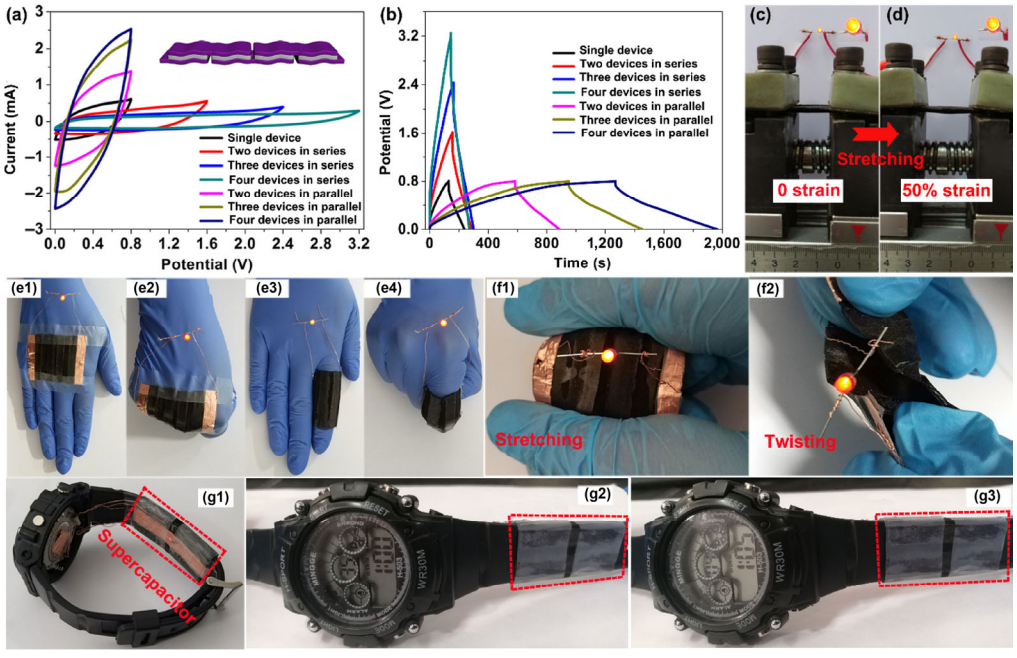

Figure 5 (a) CV and (b) GCD curves of the stretchable supercapacitor composed of multiple devices in series and parallel (scan rate = 10 $mV \cdot s^{-1}$, current density = 0.2 $A \cdot g^{-1}$). The inset is the cartoon of a stretchable supercapacitor device composed by four single devices in series. (c)–(g) Demonstrations of the stretchable supercapacitor based on the VPPyNTs/CNOs@PPyG-textile electrodes as a wearable power supply. Photographs of a red LED powered by the stretchable supercapacitor under its original (c) and stretchable states (under a strain of 50%) (d). Photographs of a red LED powered by the stretchable supercapacitor as a wearable power supply attached on the human hand and finger under the original (e1) and (e3) and stretchable states (e2) and (e4). Photographs of a red LED powered by the stretchable supercapacitor under the stretching (f1) and twisting states (f2). (g) Photographs of an electronic watch powered by a stretchable supercapacitor.

energy storage performance of the assembled supercapacitors. Our study provides a strategy to grow the vertical PPy nanotube array structure on the rough textile surface, solving the challenges of low energy storage capacitance and unstable energy storage performance in the stretchable supercapacitors.

Acknowledgements

The authors acknowledge the finance support by the National Natural Science Foundation of China (No. 51702233), the Natural Science Foundation of Tianjin City (No. 16JCYBJC41000) and support by Tianjin Key Subject for Materials Physics and Chemistry.

Electronic Supplementary Material: Supplementary material (calculation methods of specific capacitance, frequency response of capacitance, imaginary capacitance and sheet resistance; SEM and TEM images of the PPy structures; XRD profile and TEM image of the CNOs; SEM images and electrochemical performances of the PPy structures synthesized at different methyl orange concentrations; electrochemical performances of different PPy structures measured in three-electrode system; electrochemical performances of the VPPyNTs/CNOs@PPyG at different CNO concentrations; electrochemical performances of the solid-state supercapacitor devices during stretching; sheet resistance and SEM images of different PPy structures under different stretching strains; comparison of the stretchable supercapacitor performances in our work with previous reports) is available in the online version of this article at https://doi.org/10.1007/s12274-019-2360-5.

References

[1] Rogers, J. A.; Someya, T.; Huang, Y. G. Materials and mechanics for stretchable electronics. *Science* **2010**, *327*, 1603–1607.

[2] Wang, H.; Li, F. S.; Zhu, B. W.; Guo, L.; Yang, Y.; Hao, R.; Wang, H.; Liu, Y. Q.; Wang, W.; Guo, X. T. et al. Flexible integrated electrical cables based on biocomposites for synchronous energy transmission and storage. *Adv. Funct. Mater.* **2016**, *26*, 3472–3479.

[3] Kim, R. H.; Bae, M. H.; Kim, D. G.; Cheng, H. Y.; Kim, B. H.; Kim, D. H.; Li, M.; Wu, J.; Du, F.; Kim, H. S. et al. Stretchable, transparent graphene interconnects for arrays of microscale inorganic light emitting diodes on rubber substrates. *Nano Lett.* **2011**, *11*, 3881–3886.

[4] Zhao, J. X.; Li, C. W.; Zhang, Q. C.; Zhang, J.; Wang, X. N.; Sun, J.; Wang, J. J.; Xie, J. X.; Lin, Z. Y.; Li, Z. et al. Hierarchical ferric-cobalt-nickel ternary oxide nanowire arrays supported on graphene fibers as high-performance electrodes for flexible asymmetric supercapacitors. *Nano Res.* **2018**, *11*, 1775–1786.

[5] Wang, C. D.; Liu, D. B.; Chen, S. M.; Shang, Y. A.; Haleem, Y. A.; Wu, C. Q.; Xu, W. Y.; Fang, Q.; Habib, M.; Cao, J. et al. All-carbon ultrafast supercapacitor by integrating multidimensional nanocarbons. *Small* **2016**, *12*, 5684–5691.

[6] Kim, B. C.; Hong, J. Y.; Wallace, G. G.; Park, H. S. Recent progress in flexible electrochemical capacitors: Electrode materials, device configuration, and functions. *Adv. Energy Mater.* **2015**, *5*, 1500959.

[7] Jiao, X.; Zhang, C. G.; Yuan, Z. H. Facile and large-area preparation of polypyrrole film for low-haze transparent supercapacitors. *ACS Appl. Mater. Interfaces* **2018**, *10*, 41299–41311.

[8] Zhou, C. J.; Yang, Y. Q.; Sun, N.; Wen, Z.; Cheng, P.; Xie, X. K.; Shao, H. Y.; Shen, Q. Q.; Chen, X. P.; Liu, Y. N. et al. Flexible self-charging power units for portable electronics based on folded carbon paper. *Nano Res.* **2018**, *11*, 4313–4322.

[9] Huang, Y.; Tao, J. Y.; Meng, W. J.; Zhu, M. S.; Huang, Y.; Fu, Y. Q.; Gao, Y. H.; Zhi, C. Y. Super-high rate stretchable polypyrrole-based supercapacitors with excellent cycling stability. *Nano Energy* **2015**, *11*, 518–525.

[10] Zhu, J.; Tang, S. C.; Wu, J.; Shi, X. L.; Zhu, B. G.; Meng, X. K. Wearable high-performance supercapacitors based on silver-sputtered textiles with $FeCo_2S_4$-$NiCo_2S_4$ composite nanotube-built multitripod architectures as advanced flexible electrodes. *Adv. Energy Mater.* **2017**, *7*, 1601234.

[11] Bao, L. H.; Li, X. D. Towards textile energy storage from cotton T-shirts. *Adv. Mater.* **2012**, *24*, 3246–3252.

[12] Bao, Z. A.; Chen, X. D. Flexible and stretchable devices. *Adv. Mater.* **2016**, *28*, 4177–4179.

[13] Xue, Q.; Sun, J. F.; Huang, Y.; Zhu, M. S.; Pei, Z. X.; Li, H. F.; Wang, Y. K.; Li, N.; Zhang, H. Y.; Zhi, C. Y. Recent progress on flexible and wearable supercapacitors. *Small* **2017**, *13*, 1701827.

[14] Yang, Y.; Wang, H.; Hao, R.; Guo, L. Transition-metal-free biomolecule-based flexible asymmetric supercapacitors. *Small* **2016**, *12*, 4683–4689.

[15] Yue, B. B.; Wang, C. Y.; Ding, X.; Wallace, G. G. Polypyrrole coated nylon lycra fabric as stretchable electrode for supercapacitor applications. *Electrochim. Acta* **2012**, *68*, 18–24.
[16] Chen, T.; Xue, Y. H.; Roy, A. K.; Dai, L. M. Transparent and stretchable high-performance supercapacitors based on wrinkled graphene electrodes. *ACS Nano* **2014**, *8*, 1039–1046.
[17] Wang, X. L.; Hu, H.; Shen, Y. D.; Zhou, X. C.; Zheng, Z. J. Stretchable conductors with ultrahigh tensile strain and stable metallic conductance enabled by prestrained polyelectrolyte nanoplatforms. *Adv. Mater.* **2011**, *23*, 3090–3094.
[18] Wang, S. Y.; Pei, B.; Zhao, X. S.; Dryfe, R. A. W. Highly porous graphene on carbon cloth as advanced electrodes for flexible all-solid-state supercapacitors. *Nano Energy* **2013**, *2*, 530–536.
[19] Chen, B. L.; Jiang, Y. Z.; Tang, X. H.; Pan, Y. Y.; Hu, S. Fully packaged carbon nanotube supercapacitors by direct ink writing on flexible substrates. *ACS Appl. Mater. Interfaces* **2017**, *9*, 28433–28440.
[20] Zhang, N.; Luan, P. S.; Zhou, W. Y.; Zhang, Q.; Cai, L.; Zhang, X.; Zhou, W. B.; Fan, Q. X.; Yang, F.; Zhao, D. et al. Highly stretchable pseudocapacitors based on buckled reticulate hybrid electrodes. *Nano Res.* **2014**, *7*, 1680–1690.
[21] Zhang, C. G.; Peng, Z. W.; Lin, J.; Zhu, Y.; Ruan, G. D.; Hwang, C. C.; Lu, W.; Hauge, R. H.; Tour, J. M. Splitting of a vertical multiwalled carbon nanotube carpet to a graphene nanoribbon carpet and its use in supercapacitors. *ACS Nano* **2013**, *7*, 5151–5159.
[22] Yamada, T.; Namai, T.; Hata, K.; Futaba, D. N.; Mizuno, K.; Fan, J.; Yudasaka, M.; Yumura, M.; Iijima, S. Size-selective growth of double-walled carbon nanotube forests from engineered iron catalysts. *Nat. Nanotechnol.* **2006**, *1*, 131–136.
[23] Wang, K.; Wu, H. P.; Meng, Y. N.; Wei, Z. X. Conducting polymer nanowire arrays for high performance supercapacitors. *Small* **2014**, *10*, 14–31.
[24] Ni, J. F.; Li, L. Self-supported 3D array electrodes for sodium microbatteries. *Adv. Funct. Mater.* **2018**, *28*, 1704880.
[25] Zhang, C. G.; Bets, K.; Lee, S. S.; Sun, Z. Z.; Mirri, F.; Colvin, V. L.; Yakobson, B. I.; Tour, J. M.; Hauge, R. H. Closed-edged graphene nanoribbons from large-diameter collapsed nanotubes. *ACS Nano* **2012**, *6*, 6023–6032.
[26] Zhu, Y.; Li, L.; Zhang, C. G.; Casillas, G.; Sun, Z. Z.; Yan, Z.; Ruan, G. D.; Peng, Z. W.; Raji, A. R. O.; Kittrell, C. et al. A seamless three-dimensional carbon nanotube graphene hybrid material. *Nat. Commun.* **2012**, *3*, 1225.
[27] Zhang, C. G.; Li, J. J.; Zeng, X. S.; Yuan, Z. H.; Zhao, N. Q. Graphene quantum dots derived from hollow carbon nano-onions. *Nano Res.* **2018**, *11*, 174–184.
[28] Zeiger, M.; Jäckel, N.; Mochalin, V. N.; Presser, V. Review: Carbon onions for electrochemical energy storage. *J. Mater. Chem. A* **2016**, *4*, 3172–3196.
[29] Weingarth, D.; Zeiger, M.; Jäckel, N.; Aslan, M.; Feng, G.; Presser, V. Graphitization as a universal tool to tailor the potential-dependent capacitance of carbon supercapacitors. *Adv. Energy Mater.* **2014**, *4*, 1400316.
[30] Zhang, C. G.; Li, J. J.; Liu, E. Z.; He, C. N.; Shi, C. S.; Du, X. W.; Hauge, R. H.; Zhao, N. Q. Synthesis of hollow carbon nano-onions and their use for electrochemical hydrogen storage. *Carbon* **2012**, *50*, 3513–3521.
[31] Yuan, L. Y.; Yao, B.; Hu, B.; Huo, K. F.; Chen, W.; Zhou, J. Polypyrrole-coated paper for flexible solid-state energy storage. *Energy Environ. Sci.* **2013**, *6*, 470–476.
[32] Mykhailiv, O.; Imierska, M.; Petelczyc, M.; Echegoyen, L.; Plonska-Brzezinska, M. E. Chemical versus electrochemical synthesis of carbon nano-onion/polypyrrole composites for supercapacitor electrodes. *Chem.—Eur. J.* **2015**, *21*, 5783–5793.
[33] Jeong, H. T.; Kim, Y. R.; Kim, B. C. Flexible polycaprolactone (PCL) supercapacitor based on reduced graphene oxide (rGO)/single-wall carbon nanotubes (SWNTs) composite electrodes. *J. Alloys Compd.* **2017**, *727*, 721–727.
[34] Yang, X. M.; Zhu, Z. X.; Dai, T. Y.; Lu, Y. Facile fabrication of functional polypyrrole nanotubes via a reactive self-degraded template. *Macromol. Rapid Comm.* **2005**, *26*, 1736–1740.
[35] Chen, J. C.; Wang, Y. M.; Cao, J. Y.; Liu, Y.; Zhou, Y.; Ouyang, J. H.; Jia, D. H. Facile co-electrodeposition method for high-performance supercapacitor based on reduced graphene oxide/polypyrrole composite film. *ACS Appl. Mater. Interfaces* **2017**, *9*, 19831–19842.
[36] Yang, C.; Zhang, L. L.; Hu, N. T.; Yang, Z.; Wei, H.; Wang, Y. Y.; Zhang, Y. F. High-performance flexible all-solid-state supercapacitors based on densely-packed graphene/polypyrrole nanoparticle papers. *Appl. Surf. Sci.* **2016**, *387*, 666–673.
[37] Yang, J.; Wang, H.; Yang, Y.; Wu, J. P.; Hu, P. F.; Guo, L. Pseudocapacitive-dye-molecule-based high-performance flexible supercapacitors. *Nanoscale* **2017**, *9*, 9879–9885.
[38] Zhang, D.; Dong, Q. Q.; Wang, X.; Yan, W.; Deng, W.; Shi, L. Y. Preparation of a three-dimensional ordered macroporous carbon nanotube/polypyrrole composite for supercapacitors and diffusion modeling. *J. Phys. Chem. C* **2013**, *117*, 20446–20455.
[39] Song, L. F.; Zou, Y. J.; Zhang, H. T.; Xiang, C. L.; Chu, H. L.; Qiu, S. J.; Yan, E. H.; Xu, F.; Sun, L. X. High performance supercapacitor based on polypyrrole/melamine formaldehyde resin derived carbon material. *Int. J. Electrochem. Sci.* **2017**, *12*, 1014–1024.
[40] Morozan, A.; Jégou, P.; Campidelli, S.; Palacin, S.; Jousselme, B. Relationship between polypyrrole morphology and electrochemical activity towards oxygen reduction reaction. *Chem. Commun.* **2012**, *48*, 4627–4629.
[41] Li, H. H.; Song, J.; Wang, L. L.; Feng, X. M.; Liu, R. Q.; Zeng, W. J.; Huang, Z. D.; Ma, Y. W.; Wang, L. H. Flexible all-solid-state supercapacitors based on polyaniline orderly nanotubes array. *Nanoscale* **2017**, *9*, 193–200.
[42] Sultana, I.; Rahman, M. M.; Wang, J. Z.; Wang, C. Y.; Wallace, G. G.; Liu, H. K. All-polymer battery system based on polypyrrole (PPy)/para (toluene sulfonic acid) (pTS) and polypyrrole (PPy)/indigo carmine (IC) free standing films. *Electrochim. Acta.* **2012**, *83*, 209–215.
[43] Islam, N.; Warzywoda, J.; Fan, Z. Y. Edge-oriented graphene on carbon nanofiber for high-frequency supercapacitors. *Nano-Micro Lett.* **2018**, *10*, 9.
[44] Taberna, P. L.; Simon, P.; Fauvarque, J. F. Electrochemical characteristics and impedance spectroscopy studies of carbon-carbon supercapacitors. *J. Electrochem. Soc.* **2003**, *150*, A292–A300.
[45] Song, Y.; Liu, T. Y.; Xu, X. X.; Feng, D. Y.; Li, Y.; Liu, X. X. Pushing the cycling stability limit of polypyrrole for supercapacitors. *Adv. Funct. Mater.* **2015**, *25*, 4626–4632.
[46] Kovalenko, I.; Bucknall, D. G.; Yushin, G. Detonation nanodiamond and onion-like-carbon-embedded polyaniline for supercapacitors. *Adv. Funct. Mater.* **2010**, *20*, 3979–3986.
[47] Huang, J. Y.; Wang, K.; Wei, Z. X. Conducting polymer nanowire arrays with enhanced electrochemical performance. *J. Mater. Chem.* **2010**, *20*, 1117–1121.
[48] Huang, T. Q.; Cai, S. Y.; Chen, H.; Jiang, Y. Q.; Wang, S. Y.; Gao, C. Continuous fabrication of the graphene-confined polypyrrole film for cycling stable supercapacitors. *J. Mater. Chem. A* **2017**, *5*, 8255–8260.
[49] Zhang, C. G.; Ma, K.; Zhao, N. Q.; Yuan, Z. H. A core–shell strategy for improving alloy catalyst activity for continual growth of hollow carbon onions. *Cryst. Growth Des.* **2018**, *18*, 7470–7480.
[50] Noked, M.; Liu, C. Y.; Hu, J. K.; Gregorczyk, K.; Rubloff, G. W.; Lee, S. B. Electrochemical thin layers in nanostructures for energy storage. *Acc. Chem. Res.* **2016**, *49*, 2336–2346.